



# 1 A Comprehensive Characterization of Empirical Parameterizations 2 for OH Exposure in the Aerodyne Potential Aerosol Mass Oxidation 3 Flow Reactor (PAM-OFR)

4 Qianying Liu<sup>1,2</sup>, Dan Dan Huang<sup>2,\*</sup>, Andrew T. Lambe<sup>3</sup>, Shengrong Lou<sup>2</sup>, Lulu Zeng<sup>1</sup>, Yuhang Wu<sup>2</sup>,  
5 Congyan Huang<sup>2</sup>, Shikang Tao<sup>2</sup>, Xi Cheng<sup>4</sup>, Qi Chen<sup>5</sup>, Ka In Hoi<sup>1</sup>, Hongli Wang<sup>2</sup>, Kai Meng Mok<sup>1</sup>,  
6 Cheng Huang<sup>2,6</sup>, Yong Jie Li<sup>1,\*</sup>

7 <sup>1</sup>Department of Civil and Environmental Engineering, Department of Ocean Science and Technology, and Centre for Regional  
8 Oceans, Faculty of Science and Technology, University of Macau, Taipa, Macau SAR, 999078, China

9 <sup>2</sup>State Environmental Protection Key Laboratory of Formation and Prevention of Urban Air Pollution Complex, Shanghai  
10 Academy of Environmental Sciences, Shanghai, 200233, China

11 <sup>3</sup>Aerodyne Research Inc., Billerica, Massachusetts, 01821, United States

12 <sup>4</sup>School of Chemical and Environmental Engineering, China University of Mining and Technology (Beijing), Beijing 100083,  
13 China

14 <sup>5</sup>State Key Joint Laboratory of Environmental Simulation and Pollution Control, BIC-ESAT and IJRC, College of  
15 Environmental Sciences and Engineering, Peking University, Beijing, China

16 <sup>6</sup>State Ecology and Environment Scientific Observation and Research Station for the Yangtze River Delta at Dianshan Lake  
17 , Shanghai Environmental Monitoring Center, Shanghai, 200030, China

18 *Correspondence to:* Dan Dan Huang ([huangdd@saes.sh.cn](mailto:huangdd@saes.sh.cn)), Yong Jie Li ([yongjieli@um.edu.mo](mailto:yongjieli@um.edu.mo))

19 **Abstract.** The oxidation flow reactor (OFR) has been widely used to simulate secondary organic aerosol (SOA) formation in  
20 laboratory and field studies. The extent of hydroxyl radical (OH) oxidation (or OH exposure,  $\text{OH}_{\text{exp}}$ ), normally expressed as  
21 the product of OH concentration and residence time in the OFR, is important in assessing the oxidation chemistry in SOA  
22 formation. Several models have been developed to quantify the  $\text{OH}_{\text{exp}}$  in OFRs, and empirical equations have been proposed  
23 to parameterize  $\text{OH}_{\text{exp}}$ . Practically, the empirical equations and the associated parameters are derived under atmospheric  
24 relevant conditions (i.e., external OH reactivity) with limited variations of calibration conditions, such as residence time, water  
25 vapor mixing ratio,  $\text{O}_3$  concentration, etc. Whether the equations or parameters derived under limited sets of calibration  
26 conditions can accurately predict the  $\text{OH}_{\text{exp}}$  under dynamically changing experimental conditions with large variations (i.e.,  
27 extremely high external OH reactivity) in real applications remains uncertain. In this study, we conducted 62 sets of  
28 experiments (416 data points) under a wide range of experimental conditions to evaluate the scope of the application of the  
29 empirical equations to estimate  $\text{OH}_{\text{exp}}$ . Sensitivity tests were also conducted to obtain a minimum number of data points that  
30 is necessary for generating the fitting parameters. We showed that, for the OFR185 mode (185-nm lamps with internal  $\text{O}_3$   
31 generation), except for external OH reactivity, the parameters obtained within a narrow range of calibration conditions can be  
32 extended to estimate the  $\text{OH}_{\text{exp}}$  when the experiments are in wider ranges of conditions. For example, for water vapor mixing  
33 ratios, the parameters obtained within a narrow range (0.49–0.99 %) can be extended to estimate the  $\text{OH}_{\text{exp}}$  under the entire  
34 range of water vapor mixing ratios (0.49–2.76 %) studied. However, the parameters obtained when the external OH reactivity



35 is below  $23 \text{ s}^{-1}$  could not be used to reproduce the  $\text{OH}_{\text{exp}}$  under the entire range of external OH reactivity ( $4\text{--}204 \text{ s}^{-1}$ ). For the  
36 OFR254 mode (254-nm lamps with external  $\text{O}_3$  generation), all parameters obtained within a narrow range of conditions can  
37 be used to estimate  $\text{OH}_{\text{exp}}$  accurately when experimental conditions are extended, but too-low lamp voltages should be avoided.  
38 Regardless of OFR185 or OFR254 mode, at least 20–30 data points from  $\text{SO}_2$  or CO decay with varying conditions are required  
39 to fit a set of empirical parameters that can accurately estimate  $\text{OH}_{\text{exp}}$ . Caution should be exercised to use fitted parameters  
40 from low external OH reactivity to high ones, for instance, those from direct emissions such as vehicular exhaust and biomass  
41 burning.

## 42 1 Introduction

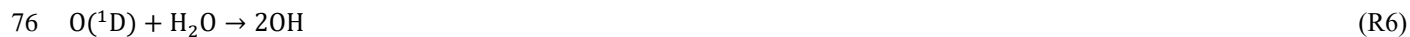
43 As the most important oxidant in tropospheric chemistry (Ehhalt, 1999), hydroxyl (OH) radical is vital in oxidizing primary  
44 pollutants such as volatile organic compounds (VOCs) and contributes to secondary organic aerosol (SOA) and tropospheric  
45 ozone ( $\text{O}_3$ ) formation. The OH radical has daytime concentrations of  $10^5$  to  $10^7$  molecules  $\text{cm}^{-3}$ , exhibiting daily (Cao et al.,  
46 2020; Tan et al., 2017), seasonal (Friedman and Farmer, 2018), as well as spatial (Cao et al., 2020; Stone et al., 2012) variations.  
47 An average daily OH radical concentration of  $1.5 \times 10^6$  molecules  $\text{cm}^{-3}$  is widely used to estimate the photochemical age of an  
48 air mass (Mao et al., 2009). Typical VOCs have second-order rate constants of  $10^{-15}$  to  $10^{-10} \text{ cm}^3 \text{ molecule}^{-1} \text{ s}^{-1}$  with OH radicals  
49 (Atkinson and Arey, 2003; Atkinson et al., 2006), which can be translated to atmospheric lifetimes of hours to approximately  
50 a year (Seinfeld and Pandis, 2016). This situation poses challenges in laboratory experiments to directly simulate the OH  
51 oxidation of VOCs, which is one of the most important chemical processes in the Earth's atmosphere.

52 Smog chambers (Cocker et al., 2001; Hildebrandt et al., 2009; Wang et al., 2014) and oxidation flow reactors (OFRs) (George  
53 et al., 2007; Kang et al., 2007; Lambe et al., 2011) have been widely employed to simulate oxidation of VOCs and subsequent  
54 SOA formation. Both types of reactors normally operate with high concentrations of oxidants (e.g., OH radicals), which lead  
55 to a significant acceleration of oxidation reactions, often by orders of magnitude. To reconcile the differences in OH  
56 concentration and exposure time between ambient and laboratory settings, the oxidation extent, i.e., OH exposure ( $\text{OH}_{\text{exp}}$ ,  
57 molecules  $\text{cm}^{-3} \text{ s}$ ) is normally used to extrapolate laboratory findings to ambient conditions. Despite drawbacks such as possible  
58 altered reaction mechanisms, this approach provides a quantitative assessment of the chemistry during OH oxidation in a  
59 reasonable time span and achievable detection capability. The  $\text{OH}_{\text{exp}}$  has a significant impact on the yield and product  
60 distribution during VOC oxidation (Cheng et al., 2021; Cheng et al., 2024). Accurate measurement or estimation of the  $\text{OH}_{\text{exp}}$   
61 during laboratory experiments, therefore, is the key to understanding the oxidation chemistry that can represent the ambient  
62 conditions.

63 The Aerodyne Potential Aerosol Mass OFR (PAM-OFR) is one of the most widely used OFRs for studying SOA formation  
64 and evolution (Zhang et al., 2024). It can achieve a wide range of atmospheric  $\text{OH}_{\text{exp}}$  conditions within short residence times  
65 on the order of minutes (Kang et al., 2007; Lambe et al., 2011). The PAM-OFR can be operated in a number of modes,  
66 depending on 1) the wavelength of the ultraviolet (UV) light source, 2) the concentration of the externally generated  $\text{O}_3$  (if



67 any), and 3) the injection of external precursor to generate  $\text{NO}_x$  ( $= \text{NO} + \text{NO}_2$ ) or other oxidants (e.g., nitrate radical or halogen  
68 atoms) upon photolysis. The most widely used methods for OH generation include combined photolysis of  $\text{O}_2$  and  $\text{H}_2\text{O}$  at  $\lambda =$   
69 185 nm plus photolysis of  $\text{O}_3$  at  $\lambda = 254$  nm (OFR185; R1–R6) or photolysis of externally added  $\text{O}_3$  at  $\lambda = 254$  nm (OFR254;  
70 R5–R6):



77 To obtain the  $\text{OH}_{\text{exp}}$  under these two modes in the PAM-OFR, one can perform decay experiments on trace gases such as  $\text{SO}_2$   
78 and  $\text{CO}$ , and fit the  $\text{OH}_{\text{exp}}$  based on known second-order rate constants between OH radical and the trace gases, which is  
79 defined as  $\text{OH}_{\text{exp, dec}}$ . Based on the results of the decay experiments, Li et al. (2015) and Peng et al. (2015) developed estimation  
80 equations to parameterize  $\text{OH}_{\text{exp}}$  as a function of easily measurable quantities, which is denoted as  $\text{OH}_{\text{exp, est}}$ . A set of parameters  
81 ( $a-f$  and  $a-c$ , respectively) for the estimation equations of the OFR185 and OFR254 modes (see Sect. 2.3 for details) were  
82 obtained by fitting the estimation equations to  $\text{OH}_{\text{exp, dec}}$  values obtained from decay experiments.

83 When using the PAM-OFR in field studies, it is necessary to obtain concurrent  $\text{OH}_{\text{exp}}$  that is representative of the ambient  
84 conditions. However, environmental conditions in field studies (e.g., humidity, temperature, etc.) are constantly changing,  
85 making it challenging to replicate these conditions for  $\text{OH}_{\text{exp}}$  estimation. In some field studies using PAM-OFR, concurrent  
86  $\text{OH}_{\text{exp}}$  was estimated by measuring the relative decay of benzene and toluene, but this requires specific instruments (Liao et  
87 al., 2021; Liu et al., 2018). To obtain accurate  $\text{OH}_{\text{exp}}$ , some studies explicitly modelled the radical chemistry in PAM-OFR (Li  
88 et al., 2015; Ono et al., 2014; Peng et al., 2015). The estimation equations developed by Li et al. (2015) and Peng et al. (2015),  
89 although empirical, reproduced the  $\text{OH}_{\text{exp}}$  from models within 10 %, making them a good choice because these equations only  
90 require the input of a few easily available parameters. Yet, it is unclear whether the fitted parameters obtained under certain  
91 conditions can still accurately estimate  $\text{OH}_{\text{exp}}$  when experimental conditions, such as UV light intensity, water vapor mixing  
92 ratio, residence time, and external OH reactivity ( $\text{OHR}_{\text{ext}}$ ), undergo significant changes. Furthermore, there is currently no  
93 consensus on the minimum number of decay experiments required to obtain accurate parameterization for  $\text{OH}_{\text{exp}}$  estimation  
94 using these equations. This facet is important for field studies using PAM-OFR where only limited numbers of decay  
95 experiments can be done to obtain concurrent  $\text{OH}_{\text{exp}}$  estimation.

96 In this study, we conducted a series of experiments using the decay of  $\text{SO}_2$  and  $\text{CO}$  to estimate the  $\text{OH}_{\text{exp}}$  in the PAM-OFR  
97 under OFR185 and OFR254 modes. The applicability of previously developed  $\text{OH}_{\text{exp}}$  estimation equations to obtain accurate



98  $\text{OH}_{\text{exp}}$  in the PAM-OFR has been evaluated by linear regression of  $\text{OH}_{\text{exp, est}}$  against  $\text{OH}_{\text{exp, dec}}$ . We have also evaluated how  
99 well estimation equations perform when using limited ranges of experimental parameters (e.g.,  $\text{OHR}_{\text{ext}}$ , residence time, water  
100 mixing ratio, etc.) or different trace gases ( $\text{SO}_2$  and CO) and given recommendations. In addition, we have proposed the  
101 minimal number of trace-gas decay experiments required to obtain a set of usable parameters for the  $\text{OH}_{\text{exp}}$  estimation  
102 equations. Finally, we also compared the advantages and disadvantages of the OFR185 and the OFR254 modes from the  
103 perspective of the quantification of  $\text{OH}_{\text{exp}}$ . The methodology of this study can be applied to laboratory and field experiments  
104 for  $\text{OH}_{\text{exp}}$  estimation using PAM-OFR or other OFRs for OH oxidation chemistry.

## 105 **2 Methods**

### 106 **2.1 The PAM-OFR**

107 Experiments were conducted using an Aerodyne PAM-OFR (Aerodyne Research Inc., Billerica, MA, US), which is a  
108 horizontal aluminium cylindrical chamber with an internal volume of 13.3 L. The PAM-OFR operates in a continuous flow  
109 mode. Four low-pressure Hg lamps are installed inside the reactor to produce UV light with characteristic spectral lines (e.g.,  
110 185 and 254 nm). The OH was generated via OFR185 using two ozone-producing Hg lamps (GPH436T5VH/4P, Light  
111 Sources, Inc.) or via OFR254 using two ozone-free Hg lamps (GPH436TL/4P, Light Sources, Inc.) to photolyze externally  
112 added ozone. A flow of nitrogen purge gas, ranging from 0.2 to 0.3 L  $\text{min}^{-1}$ , is introduced between the lamps and sleeves. This  
113 nitrogen gas flow serves to reduce the heat generated by the lamps and prevent the formation and accumulation of ozone  
114 between the lamps and the quartz tubes that isolate them from the sample flow in the OFR. A fluorescent dimming ballast is  
115 used to control the photon flux by regulating the voltage applied to the lamps, which allows us to generate different OH  
116 concentrations. In typical measurement sequences, nine lamp voltage settings (including lights off) were cycled through every  
117 2–3 hours. The dimming voltage ranged from 0 to 10 V direct current (DC).

### 118 **2.2 $\text{OH}_{\text{exp}}$ estimation through decay of $\text{SO}_2$ and CO ( $\text{OH}_{\text{exp, dec}}$ )**

119 Inorganic trace gases  $\text{SO}_2$  or CO react with OH radicals at slower rates compared to most VOCs. However, considering the  
120 complex oxidation chemistry of VOCs,  $\text{SO}_2$  and CO can better capture the features of real  $\text{OHR}_{\text{ext}}$  decay and effective  $\text{OHR}_{\text{ext}}$   
121 (Peng et al., 2015). We performed systematic decay experiments with  $\text{SO}_2$  and CO in the PAM-OFR, with conditions tabulated  
122 in Tables S1 and S2. Figure S1 shows the schematics of the experimental setups in the OFR185 and OFR254 modes. In the  
123 OFR185 mode, the injected gas flow at the inlet of the PAM is made up of three sub-flows: (1) The trace-gas flow, i.e.  $\text{SO}_2$  of  
124 0.2–8.7 ppm or CO of 10.2–207.5 ppm supplied from gas cylinders (Shanghai Shenkai Gases Technology CO., LTD.); (2) dry  
125 clean air from a zero-air generator (ZAS-100/150, Convenient) with a total hydrocarbon content of less than 0.1 ppm; (3) the  
126 humidified clean air passed through a Nafion humidifier (FC100-80-6MSS, Perma Pure). By adjusting the ratio of dry air to  
127 humidified air, the water vapor mixing ratio in the PAM-OFR can be controlled. Additionally, they also serve as makeup flows



128 to maintain a constant flow rate. At the outlet of the reactor, the gas flow was sampled from an internal perforated Teflon ring.  
129 The gas-phase species ( $\text{O}_3$ ,  $\text{SO}_2$ , and  $\text{CO}$ ) were detected using an ultraviolet ozone analyser (UV-100, Eco Sensors), an  $\text{SO}_2$   
130 monitor (Model 43i, Thermo Scientific), and a  $\text{CO}$  monitor (G2401, Picarro), respectively. In the OFR254 mode, in addition  
131 to the previously mentioned setup, externally generated  $\text{O}_3$  (through UV photolysis) with desired concentrations was injected  
132 at the inlet of the PAM-OFR.

133 Figures S2a and S2b depict examples of set and measured parameters during experiments conducted in the OFR185 and  
134 OFR254 modes, respectively. In the OFR185 mode, the tracer species concentration was allowed to stabilize under dark  
135 conditions. Once the concentration reached a steady state, the UV lamps were turned on. Different light intensities lead to  
136 varying levels of decay of  $\text{SO}_2$  or  $\text{CO}$  after oxidation, reflecting different  $\text{OH}_{\text{exp}}$  within the PAM-OFR. In the OFR254 mode,  
137 it is necessary to obtain the initial concentration of  $\text{O}_3$  injected into the PAM-OFR in the absence of  $\text{OHR}_{\text{ext}}$ . While waiting for  
138 the  $\text{SO}_2$  or  $\text{CO}$  concentration to stabilize, the  $\text{O}_3$  flow was temporarily blocked outside the PAM-OFR using a valve. Dry clean  
139 air was then introduced to compensate for this portion of the flow, ensuring a constant total flow throughout the entire process.  
140 Once the tracer species concentration had reached a steady state, the  $\text{O}_3$  was then allowed to flow into the PAM-OFR. The  
141 total  $\text{OH}_{\text{exp, dec}}$  in the reactor was varied over a wide range (approximately  $10^9$ – $10^{12}$  molecules  $\text{cm}^{-3}$  s) by changing the UV  
142 light intensity, water mixing ratio, and residence time. The mean residence time was obtained from the ratio of the internal  
143 volume of and the total flow rate through the PAM-OFR. In the calculation of  $\text{OH}_{\text{exp, dec}}$  (see the paragraph below), plug flow  
144 conditions were assumed, which has been shown to agree with the residence time distribution (RTD) approach for  $\text{OH}_{\text{exp}}$  by  
145 Li et al. (2015) and Peng et al. (2015).

146  $\text{OH}_{\text{exp, dec}}$  in the PAM-OFR was calculated from the pseudo-first-order reaction of OH with  $\text{SO}_2$  or  $\text{CO}$ , whose reaction rate  
147 constants with OH radicals have been well characterized ( $k_{\text{SO}_2, \text{OH}} = 9.49 \times 10^{-13}$   $\text{cm}^3$  molecule $^{-1}$  s $^{-1}$  and  $k_{\text{CO, OH}} = 2.4 \times 10^{-13}$   
148  $\text{cm}^3$  molecule $^{-1}$  s $^{-1}$  at 1 atm and 298 K) (Burkholder et al., 2020; Cao et al., 2020). By measuring the decay of  $\text{SO}_2$  or  $\text{CO}$ , the  
149 corresponding  $\text{OH}_{\text{exp, dec}}$  is calculated as follows:

$$150 \quad \text{OH}_{\text{exp, dec}} = \frac{-1}{k_{i, \text{OH}}} \times \ln \left( \frac{c_{i, \text{out}}}{c_{i, \text{in}}} \right) \quad (1)$$

151 where  $c_{i, \text{in}}$  is the concentration of reactant  $i$  injected into the PAM-OFR (ppb),  $c_{i, \text{out}}$  is reactant  $i$  concentration at the PAM-  
152 OFR outlet (ppb), and  $k_{i, \text{OH}}$  is the second-order rate constant between the trace species ( $\text{SO}_2$  or  $\text{CO}$ ) and OH radicals.

### 153 **2.3 $\text{OH}_{\text{exp}}$ estimation from empirical equations ( $\text{OH}_{\text{exp, est}}$ )**

154 Li et al. (2015) proposed an  $\text{OH}_{\text{exp, est}}$  estimation equation (Eq. 2) for OFR185 based on easily measurable quantities:

$$155 \quad \text{OH}_{\text{exp, est}} = 10^{[a + (b + c \times \text{OHR}_{\text{ext}}^d + e \times \log(\text{O}_{3, \text{out}} \times \frac{180}{t}) \times \text{OHR}_{\text{ext}}^f) \times \log(\text{O}_{3, \text{out}} \times \frac{180}{t}) + \log \text{H}_2\text{O} + \log(\frac{t}{180})]} \quad (2)$$

156 where  $a$ – $f$  are fitting parameters (values are reported in Table S3);  $\text{O}_{3, \text{out}}$  is ozone concentration measured at the exit of the  
157 PAM-OFR (molecules  $\text{cm}^{-3}$ ), which serves as a surrogate for UV flux;  $\text{H}_2\text{O}$  is water vapor mixing ratio in PAM-OFR (%);  $t$  is



158 mean residence time (s). The total external OH reactivity is represented by  $\text{OHR}_{\text{ext}} (\text{s}^{-1}) = \sum_i k_i [C_i]$ , where  $k_i$  and  $[C_i]$  are the  
159 rate constants with OH and the concentration of the OH-consuming reactant  $i$  in the system (Wang et al., 2020).

160 Peng et al. (2015) proposed another equation (Eq. (3)) for  $\text{OH}_{\text{exp, est}}$  in OFR254:

$$161 \quad \text{OH}_{\text{exp, est}} = 10^{\left[ a + \log(-\log r_{\text{O}_3}) + b \times \left( \frac{\text{OHR}_{\text{ext}}}{\text{O}_{3, \text{in}}} \right)^c \right]} \quad (3)$$

162 where  $a$ – $c$  are fitting parameters (values are reported in Table S4);  $\log r_{\text{O}_3}$  ( $\log (\text{O}_{3, \text{out}}/\text{O}_{3, \text{in}})$ ) is the logarithm of the ratio  
163 between the output and input  $\text{O}_3$  concentrations, which serves as a surrogate for UV flux and also captures the effect of  $\text{H}_2\text{O}$ ;  
164  $\text{O}_{3, \text{in}}$  is the concentration of externally injected  $\text{O}_3$  into the PAM-OFR (molecules  $\text{cm}^{-3}$ ).

165 We have performed in total of 62 sets of trace-gas decay experiments with 416 data points for the  $\text{OH}_{\text{exp, dec}}$ , with 25 sets and  
166 175 data points in the OFR185 mode and 37 sets and 241 data points in the OFR254 mode. After obtaining the  $\text{OH}_{\text{exp, dec}}$  values,  
167 we used Eqs. 2 and 3 to fit the parameters  $a$ – $f$  and  $a$ – $c$  for OFR185 and OFR254 modes, respectively, given that the  
168 experimental parameters such as  $\text{OHR}_{\text{ext}}$ ,  $\text{O}_{3, \text{out}}$ ,  $\text{H}_2\text{O}$ , and  $t$  (in Eq. 2), and  $r_{\text{O}_3}$ ,  $\text{OHR}_{\text{ext}}$ , and  $\text{O}_{3, \text{in}}$  (in Eq. 3) are known. The  
169  $\text{OH}_{\text{exp, est}}$  values were then reconstructed with the fitted parameters and the experimental parameters, and compared with the  
170  $\text{OH}_{\text{exp, dec}}$  values via linear regression analysis. The generation of OH radicals in PAM-OFR is related to the photon fluxes at  
171  $\lambda = 185 \text{ nm}$  ( $I_{185}$ ) and  $\lambda = 254 \text{ nm}$  ( $I_{254}$ ). According to Rowe et al. (2020),  $I_{185}:I_{254}$  is specific to the Hg lamp utilized. Since the  
172  $\text{OH}_{\text{exp}}$  estimation equation for OFR185 uses  $\text{O}_3$  concentration as a measurable surrogate for the UV flux at 185 nm, it is also  
173 lamp-specific. Because the UV lamps used in our study are different from the BHK lamps employed by Li et al. (2015), we  
174 anticipate that the parameters  $a$ – $f$  fitted from our decay experiments (Table S3) should be quite different from those in Li et al.  
175 (2015), which is indeed the case. Similarly, fitted parameters  $a$ – $c$  for OFR254 mode from our decay experiments (Table S4)  
176 are also different from those in Peng et al. (2015).

## 177 **3 Results and Discussion**

### 178 **3.1 The OFR185 mode: $\text{OHR}_{\text{ext}}$ level relevant to ambient conditions**

179 Field studies showed that the environmental  $\text{OHR}_{\text{ext}}$  mainly fluctuated between 10–30  $\text{s}^{-1}$  (Fuchs et al., 2017; Lou et al., 2010;  
180 Lu et al., 2010; Tan et al., 2018; Yang et al., 2017). To investigate the factors that potentially affect the fitting parameters of  
181 Eq. 2 in the estimation of  $\text{OH}_{\text{exp}}$  under ambient conditions, we first performed 16 sets of experiments with  $\text{OHR}_{\text{ext}}$  of 4–23  $\text{s}^{-1}$   
182 using  $\text{SO}_2$  as the  $\text{OHR}_{\text{ext}}$  source. With the measured  $\text{OH}_{\text{exp, dec}}$ , the parameters ( $a$ – $f$ ) were first derived, which were used to  
183 reconstruct  $\text{OH}_{\text{exp, est}}$  using Eq. 2 with known  $\text{OHR}_{\text{ext}}$ , ozone concentration ( $\text{O}_{3, \text{out}}$ ), water vapor mixing ratio ( $\text{H}_2\text{O}$ ), and  
184 residence time ( $t$ ). The reconstructed  $\text{OH}_{\text{exp, est}}$  values were plotted against the  $\text{OH}_{\text{exp, dec}}$  values calculated from the trace-gas  
185 decay experiments, as shown in Figure 1.

186 We first investigated the effect of changing residence time on the  $\text{OH}_{\text{exp}}$  estimation. With other experimental parameters (i.e.  
187  $\text{H}_2\text{O}$ ,  $\text{O}_{3, \text{out}}$ , and  $\text{OHR}_{\text{ext}}$ ) being similar, we set the residence time to a low value (33 s) and also a range of higher values (61–



188 199 s). With the residence time of 33 s, the reconstructed  $\text{OH}_{\text{exp, est}}$  correlates well with the experimental  $\text{OH}_{\text{exp, dec}}$  (slope =  
189 1.061 and  $R^2 = 0.990$ , Figure 1a1). The set of fitted parameters  $a-f$  ( $\text{FP}_{\text{st, 185}}$ ; st: short time) applied in Figure 1a1 is presented  
190 in Table S3. When the residence time was increased to 61–199 s, the interpolated  $\text{OH}_{\text{exp, est}}$  utilizing  $\text{FP}_{\text{st, 185}}$  was also in good  
191 correlation with  $\text{OH}_{\text{exp, dec}}$  (slope = 0.978,  $R^2 = 0.959$ , Figure 1a2). We also derived fitted parameters ( $\text{FP}_{\text{et, 185}}$ ; et: extended t)  
192 using the data points with the extended range of residence time (33–199 s). Not surprisingly, with the application of  $\text{FP}_{\text{et, 185}}$ ,  
193  $\text{OH}_{\text{exp, est}}$  also correlated well with  $\text{OH}_{\text{exp, dec}}$  (slope = 0.994,  $R^2 = 0.955$ , Figure 1a3). The results indicate that variation in  
194 residence time does not significantly affect the fitting parameters of Eq. 2 for the  $\text{OH}_{\text{exp}}$  estimation. From an experimental  
195 perspective, since  $\text{OH}_{\text{exp}}$  is the product of OH radical concentration ( $[\text{OH}]$ ) and the residence time (t), as long as the change of  
196 t does not significantly alter the quasi-steady-state  $[\text{OH}]$ , the fitted parameters from a narrow range of t should be applicable  
197 to situations of longer t. Mathematically, two terms of  $180/t$  and  $t/180$  are related to t, ranging from 0.90–5.45 and 0.18 to 1.11,  
198 respectively, which do not contribute significantly to the exponent in Eq. 2 after taking the logarithm of them. Avery et al.  
199 (2023) also arrived at a similar conclusion. They showed that the estimation of  $\text{OH}_{\text{exp}}$  using fitted parameters from another  
200 study (Rowe et al., 2020) differed by only  $\pm 50\%$  with a slight change of residence time.

201 Similarly, we then investigated the impacts of  $\text{H}_2\text{O}$  on the estimation of  $\text{OH}_{\text{exp}}$ . Applying fitted parameters from experiments  
202 of low water vapor mixing ratios (0.49–0.99 %, Figure 1b1) ( $\text{FP}_{\text{IH}_2\text{O, 185}}$ ;  $\text{IH}_2\text{O}$ : low  $\text{H}_2\text{O}$ ) to data spanning a wide range of  
203 water vapor mixing ratios (0.49–2.76 %) also yielded a reasonably good correlation between  $\text{OH}_{\text{exp, est}}$  and  $\text{OH}_{\text{exp, dec}}$  (Figure  
204 1b2). This could be attributed to the fact that the term  $\log\text{H}_2\text{O}$  in Eq. 2 does not contribute significantly to the exponent.

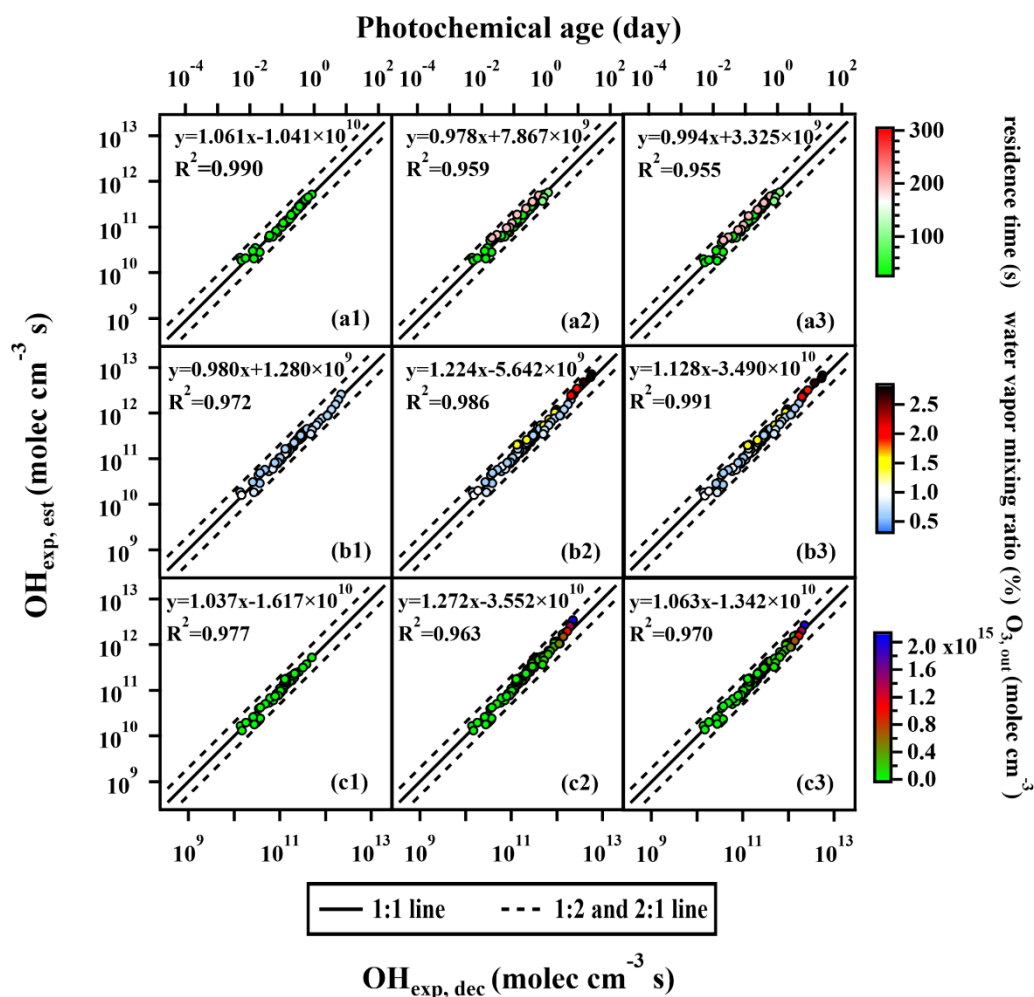
205 As for ozone concentration, applying fitting parameters ( $\text{FP}_{\text{IO}_3, 185}$ ;  $\text{IO}_3$ : low  $\text{O}_{3, \text{out}}$ ) from experiments of low ozone  
206 concentration ( $1.44 \times 10^{12}$ – $6.79 \times 10^{13}$  molecules  $\text{cm}^{-3}$ , Figure 1c1) to reconstruct the data for a wide range ( $1.44 \times 10^{12}$ – $2.03$   
207  $\times 10^{15}$  molecules  $\text{cm}^{-3}$ ) yielded a reasonably good correlation between  $\text{OH}_{\text{exp, est}}$  and  $\text{OH}_{\text{exp, dec}}$  (Figure 1c2). It only resulted in  
208 a mildly increased slope (from 1.063 to 1.272) and similar  $R^2$  values (both are 0.970) as compared to those using the whole  
209 ozone concentration range (Figure 1c3).

210 Ideally, trace-gas decay experiments covering the entire ranges of the t,  $\text{H}_2\text{O}$ , and  $\text{O}_{3, \text{out}}$  variations under real experimental  
211 conditions should be conducted, which is labor-intensive. Practically, due to the atmospherically relevant variations that occur  
212 in t,  $\text{H}_2\text{O}$ , and  $\text{O}_{3, \text{out}}$  during the real experiments, the ranges of t,  $\text{H}_2\text{O}$ , and  $\text{O}_{3, \text{out}}$  covered by trace-gas decay experiments are  
213 usually narrower compared to the real experiments. Our results suggest that the fitting parameters ( $a-f$ ) obtained from  
214 calibration experiments with relatively narrow ranges of t,  $\text{H}_2\text{O}$ , and  $\text{O}_{3, \text{out}}$  can still provide a reliable estimation of OH radical  
215 levels during the real experiments, which would cover wider ranges of these conditions.

216 It is noteworthy that reliable estimations can be achieved regardless of whether the narrow range is situated within the lower  
217 or higher interval of the full condition range. Figure 1 demonstrated the case where the narrow range was situated within the  
218 lower interval, while Figure S3 presented the case where the narrow range was situated within the higher interval. As shown  
219 in Figure S3, the data points in panel a1 had residence times of 100–296 s, the data points in panel b1 had water vapor mixing  
220 ratios of 1.04–2.76 %, and the data points in panel c1 had  $\text{O}_{3, \text{out}}$  of  $8.45 \times 10^{13}$ – $2.03 \times 10^{15}$  molecules  $\text{cm}^{-3}$ . Panels a2, b2, and  
221 c2 built on panels a1, b1, and c1 by incorporating data points with shorter t (33–61 s), lower  $\text{H}_2\text{O}$  (0.49–0.97 %), and lower



222  $O_{3, \text{out}}$  ( $1.44 \times 10^{12}$ – $6.79 \times 10^{13}$  molecules  $\text{cm}^{-3}$ ), respectively, but still used fitting parameters  $a$ – $f$  obtained from the higher  
 223 range of conditions to estimate  $\text{OH}_{\text{exp, est}}$ . In panels a3, b3, and c3, the parameters  $a$ – $f$  were refitted using all the data points  
 224 included in the expanded  $t$ ,  $\text{H}_2\text{O}$ , and  $O_{3, \text{out}}$  ranges, respectively, and the obtained  $a$ – $f$  were used to estimate  $\text{OH}_{\text{exp, est}}$ . Using  
 225 panel a1–a3 in Figure S3 as an example, the slope and  $R^2$  values in a2 and a3 were very close to 1, reflecting the good  
 226 consistency between  $\text{OH}_{\text{exp, est}}$  and  $\text{OH}_{\text{exp, dec}}$ . In the OFR254 mode discussed later (Figure 4, panels c1–c3), this narrower range  
 227 can also be situated within the middle interval of the full condition range. This applicability of fitting parameters obtained from  
 228 narrow ranges of experimental conditions is beneficial for quickly obtaining concurrent  $\text{OH}_{\text{exp}}$  during the experiments in field  
 229 measurements.



230

231 **Figure 1:** The regression results of  $\text{OH}_{\text{exp, est}}$  and  $\text{OH}_{\text{exp, dec}}$  when variations occurred in (a1–a3) residence time, (b1–b3) water vapor  
 232 mixing ratio, and (c1–c3) output  $O_3$  concentration under atmospheric relevant  $\text{OHR}_{\text{ext}}$  level ( $4$ – $23 \text{ s}^{-1}$ ). Compared to panels a1, b1,  
 233 and c1, panels a2, b2, and c2 respectively incorporated additional data points with higher  $t$ ,  $\text{H}_2\text{O}$ , and  $O_{3, \text{out}}$  values, but still utilized  
 234 the fitting parameters  $\text{FP}_{\text{st}, 185}$ ,  $\text{FP}_{\text{H}_2\text{O}, 185}$ , and  $\text{FP}_{\text{O}_3, 185}$  obtained from the lower condition range to estimate  $\text{OH}_{\text{exp, est}}$ . In panels a3,





235 **b3, and c3, all data points within the extended condition range were used to re-fit the parameters  $a-f$ , and the resulting  $FP_{et, 185}$ ,**  
236  **$FP_{eH_2O, 185}$ , and  $FP_{eO_3, 185}$  were employed to estimate  $OH_{exp, est}$  (s: short, l: low, e: extended).**

### 237 **3.2 The OFR185 mode: $OHR_{ext}$ level relevant to emission sources**

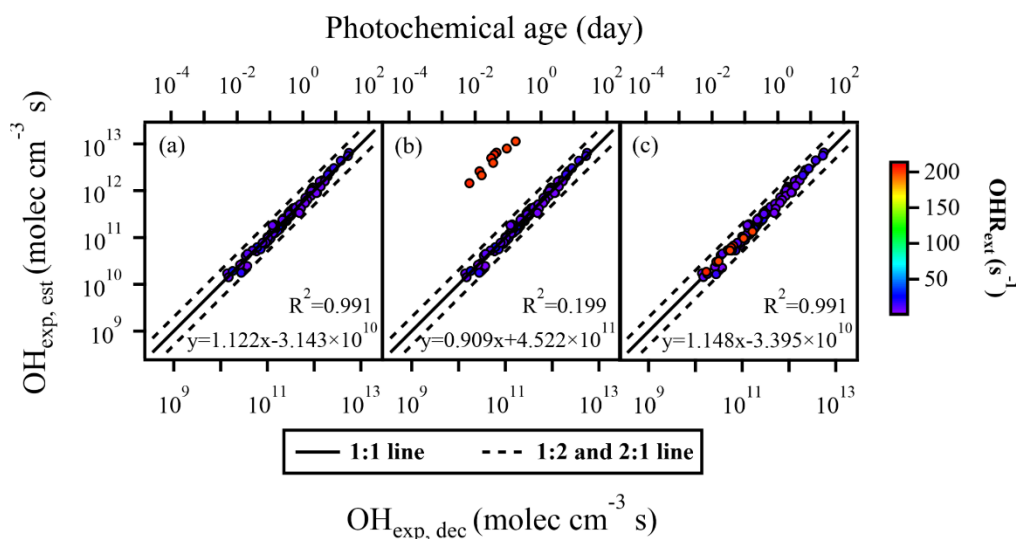
238 The experimental conditions in the PAM-OFR often involve not only general atmospheric conditions ( $OHR_{ext} < 30 \text{ s}^{-1}$ ) but  
239 also high-concentration conditions, e.g., those directly from emission sources. For instance, the  $OHR_{ext}$  of direct vehicle  
240 emission can be as high as  $1000 \text{ s}^{-1}$  with plenty of reducing gases such as CO and VOCs (Nakashima et al., 2010). To evaluate  
241 the applicability of Eq. 2 under situations of high  $OHR_{ext}$ , we performed high  $OHR_{ext}$  (up to  $204 \text{ s}^{-1}$ ) experiments using high  
242 concentrations of  $SO_2$  as the  $OHR_{ext}$  source. Compared to the data points shown in Figure 2a ( $4-23 \text{ s}^{-1}$ ), Figure 2b and Figure  
243 2c included additional data points with higher  $OHR_{ext}$  values ( $198-204 \text{ s}^{-1}$ ), while the other conditions remained similar. In  
244 Figure 2b, the parameters  $a-f$  ( $FP_{IOHR, 185}$ ; IOHR: low  $OHR_{ext}$ ) obtained from the low- $OHR_{ext}$  data points were used to estimate  
245  $OH_{exp, est}$ , yet those used in Figure 2c were refitted from the data points with extended  $OHR_{ext}$  range ( $4-204 \text{ s}^{-1}$ ). It could be  
246 observed from Figure 2b that when estimating  $OH_{exp}$  using  $FP_{IOHR, 185}$ ,  $OH_{exp, est}$  of the high- $OHR_{ext}$  data points were  
247 significantly overestimated, with a difference of more than two orders of magnitudes compared to  $OH_{exp, dec}$ . This observation  
248 suggests that, different from cases for residence time, water vapor mixing ratio, and ozone concentration shown in the section  
249 above,  $FP_{IOHR, 185}$  were not applicable to high- $OHR_{ext}$  conditions.

250 We then investigated the possible causes of the discrepancy for  $OH_{ext}$  estimation between  $FP_{IOHR, 185}$  and  $FP_{eOHR, 185}$ . According  
251 to Eq. 2, the third term  $c \times OHR_{ext}^d \times \log(O_{3, out} \times 180/t)$  and the fourth term  $e \times OHR_{ext}^f \times [\log(O_{3, out} \times 180/t)]^2$  are associated  
252 with  $OHR_{ext}$ , which involve fitted parameters of  $c-f$ . To investigate their relationships with  $OHR_{ext}$ , we performed a sensitivity  
253 test with a fixed ozone concentration ( $1.77 \times 10^{14} \text{ molecules cm}^{-3}$ ) and residence time (89 s), which were mean values during  
254 our experiments. When using the  $c-f$  values of  $FP_{IOHR, 185}$  ( $-0.13922$ ,  $0.26786$ ,  $0.0026332$ , and  $0.4917$ ), the variations of the  
255 third term, the fourth term, and their sum with respect to  $OHR_{ext}$  were shown in Figure S4a1–a3, respectively. The third term  
256 (Figure S4a1) was negative and decreased as  $OHR_{ext}$  increased, while the fourth term (Figure S4a2) was positive and increased  
257 as  $OHR_{ext}$  increased. The sum of them (Figure S4a3), however, first decreased and then started to increase at approximately  
258  $OHR_{ext} = 21 \text{ s}^{-1}$ , owing possibly to a slower decrease in the third term or a faster increase in the fourth. If contributions from  
259 other terms in Eq. 2 were constant, this led to an increase of  $OH_{exp}$  as  $OHR_{ext}$  increased beyond  $21 \text{ s}^{-1}$ . Our results showed that  
260 the expectation that  $OH_{exp}$  should decrease with increasing  $OHR_{ext}$  (Li et al., 2015) was applicable to the lower ranges of  
261  $OHR_{ext}$ , i.e., under atmospheric relevant conditions. With further increase of  $OHR_{ext}$ , i.e., above atmospheric relevant condition,  
262 the fitted parameters obtained from the dataset with  $FP_{IOHR, 185}$  were not applicable.

263 When using the  $c-f$  values of  $FP_{eOHR, 185}$  ( $-0.079114$ ,  $0.36805$ ,  $0.0041654$ , and  $0.38722$ ), the trends of the third and the fourth  
264 terms (Figure S4b1 and S4b2, respectively) were similar to those with low  $OHR_{ext}$  (Figure S4a1 and S4a2, respectively); their  
265 sum, however, gave a monotonical decreasing trend as  $OHR_{ext}$  increased (Figure S4b3), consistent with the expectation that  
266  $OH_{exp}$  should decrease with increasing  $OHR_{ext}$  (Li et al., 2015).



267 Nevertheless, the good agreement between  $\text{OH}_{\text{exp, est}}$  and  $\text{OH}_{\text{exp, dec}}$  in Figure 2c (using re-fitted parameters from the dataset of  
268 extended  $\text{OHR}_{\text{ext}}$ ) indicate that Eq. 2 can still be used to estimate  $\text{OH}_{\text{exp}}$  under high- $\text{OHR}_{\text{ext}}$  conditions. This conclusion is  
269 further supported by the results of  $\text{OH}_{\text{exp}}$  obtained using CO as the  $\text{OHR}_{\text{ext}}$  source (see Figure 3 and the section below) under  
270 extremely high- $\text{OHR}_{\text{ext}}$  conditions (up to  $1200 \text{ s}^{-1}$ ). This is advantageous for the use of PAM-OFR in simulations of SOA  
271 formation from direct emission sources (e.g., vehicular exhaust and biomass burning) where  $\text{OHR}_{\text{ext}}$  is extremely high. It is,  
272 however, desirable to have  $\text{OH}_{\text{exp}}$  estimated under similarly high  $\text{OHR}_{\text{ext}}$  for those experiments to accurately represent the  
273 extent of oxidation.



274

275 **Figure 2: The regression results of  $\text{OH}_{\text{exp, est}}$  and  $\text{OH}_{\text{exp, dec}}$  with different  $\text{OHR}_{\text{ext}}$  levels. In panel a, data points with atmospheric**  
276 **relevant  $\text{OHR}_{\text{ext}}$  level ( $4\text{--}22 \text{ s}^{-1}$ ) were applied. In addition to the data points contained within panel a, panel b included additional**  
277 **data points with emission sources related  $\text{OHR}_{\text{ext}}$  level ( $198\text{--}204 \text{ s}^{-1}$ ), but  $\text{FP}_{\text{IOHR, 185}}$  were still used to estimate  $\text{OH}_{\text{exp, est}}$ . The data**  
278 **points in panel c were identical to those in panel b, but the estimation of  $\text{OH}_{\text{exp, est}}$  utilized the  $\text{FP}_{\text{eOHR, 185}}$  obtained by fitting all data**  
279 **points across the full range of  $\text{OHR}_{\text{ext}}$  levels.**

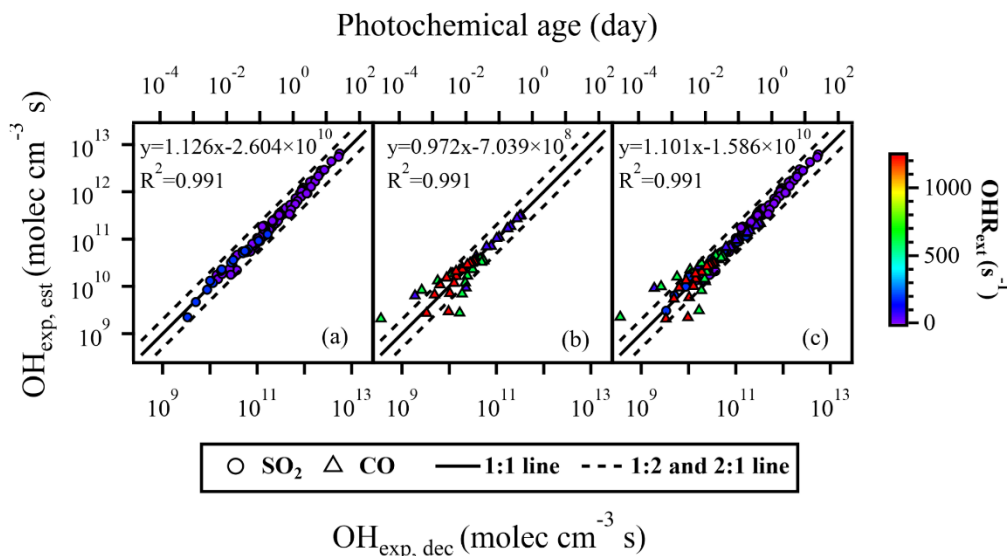
### 280 3.3 The OFR185 mode: $\text{SO}_2$ and CO as $\text{OHR}_{\text{ext}}$ sources

281 Peng et al. (2015) suggested that  $\text{SO}_2$  can better capture the features of real  $\text{OHR}_{\text{ext}}$  decay and effective  $\text{OHR}_{\text{ext}}$ . The reaction  
282 between  $\text{SO}_2$  and OH is relatively straightforward and is not expected to undergo too many side reactions. CO is a typical  
283 gaseous inorganic compound emitted during combustion process. Using CO as an  $\text{OHR}_{\text{ext}}$  source to explore the estimation of  
284  $\text{OH}_{\text{exp}}$  in the simulation of oxidation chemistry for emission sources (i.e., high  $\text{OHR}_{\text{ext}}$  level) is representative. Therefore, we  
285 compared the results with  $\text{SO}_2$  (Figure 3a) and CO (Figure 3b) as the  $\text{OHR}_{\text{ext}}$  source. When using  $\text{SO}_2$  as the  $\text{OHR}_{\text{ext}}$  source,  
286 all data points agreed within a factor of 2 (Figure 3a). while only approximately 83 % of the data points agreed within a factor  
287 of 2 when CO was used as the  $\text{OHR}_{\text{ext}}$  source (Figure 3b). The deviating data points were mostly concentrated in areas with  
288 high  $\text{OHR}_{\text{ext}}$  ( $> 600 \text{ s}^{-1}$ ) and low  $\text{O}_3, \text{out}$  concentration ( $10^{12}\text{--}10^{13} \text{ molecules cm}^{-3}$ ), where the removal of CO was relatively low.  
289 Li et al. (2015) have observed increased deviations between  $\text{OH}_{\text{exp, est}}$  and  $\text{OH}_{\text{exp, dec}}$ , which was attributed, at least in part, to



290 the increased measurement uncertainties for CO when the decrease of its concentration was marginal. We believe that  
291 measurement uncertainty might not be the main reason in our case, because most of the decreases in CO concentration during  
292 our experiments were larger than the precision of the Picarro G2401 Analyzer (~1.5 ppb at 5 min time resolution). Another  
293 possible reason is that in addition to the reaction with OH radicals, CO may react with some other oxidants, leading to its  
294 consumption, while SO<sub>2</sub> was less affected, thereby resulting in more scattered data points for CO. The reaction rate of CO with  
295 HO<sub>2</sub> is very slow, and is unlikely to play a significant role ( $k_{\text{CO, HO}_2} = 5.55 \times 10^{-27} \text{ cm}^3 \text{ molecule}^{-1} \text{ s}^{-1}$  at 300 K) (You et al.,  
296 2007). Cohen and Heicklen (1972) suggested that CO could also react with atomic oxygen (O(<sup>1</sup>D)). Clerc and Barat (1967)  
297 have reported some appreciable rate coefficients ( $10^{-11}$  to  $10^{-12} \text{ cm}^3 \text{ molecule}^{-1} \text{ s}^{-1}$ ) for the reaction between CO and O(<sup>1</sup>D),  
298 which are higher than those for the reactions of CO with OH ( $k_{\text{CO, OH}} = 2.4 \times 10^{-13} \text{ cm}^3 \text{ molecule}^{-1} \text{ s}^{-1}$  at 298 K) (Burkholder et  
299 al., 2020). It is therefore possible that reaction between CO and O(<sup>1</sup>D) might have complicated the decay of CO in the PAM-  
300 OFR. To further investigate this aspect, we used the KinSim, a kinetic simulator, to calculate the average mixing ratios of OH,  
301 O(<sup>1</sup>D), and HO<sub>2</sub> under the specific conditions in the PAM-OFR, and then assessed the relative importance of the reactions CO  
302 + OH → CO<sub>2</sub> + H, CO + O(<sup>1</sup>D) → CO<sub>2</sub>, and CO + HO<sub>2</sub> → CO<sub>2</sub> + OH (Li et al., 2015; Peng and Jimenez, 2019, 2020). The  
303 results show that although the reaction rate constant of CO and O(<sup>1</sup>D) is 1–2 orders of magnitude higher than that of CO and  
304 OH, the concentration of OH is about 6–7 orders of magnitude higher than the concentration of O(<sup>1</sup>D), indicating that the  
305 reaction of CO with O(<sup>1</sup>D) will not have a significant impact on the consumption of CO. The real reason for the scattered data  
306 points when using CO in the trace-gas decay experiment is still unknown.

307 Figure 3c includes the results of trace-gas decay experiments using both SO<sub>2</sub> and CO as the OHR<sub>ext</sub> source. Despite having  
308 different reaction rates with OH radicals, the data points could be collectively utilized to fit the parameters for the estimation  
309 equation. With approximately 95 % of the results agreeing within a factor of 2, OH<sub>exp, est</sub> obtained using the fitted parameters  
310 exhibited good agreements (slope = 1.101, R<sup>2</sup> = 0.991) with OH<sub>exp, dec</sub>. Our results thus suggest that although using CO as the  
311 OHR<sub>ext</sub> might result in some scattered data points, it was still feasible to use Eq. 2 to estimate OH<sub>exp</sub> given that experiments  
312 were not done solely in conditions with high OHR<sub>ext</sub> (i.e., high CO concentrations) and low O<sub>3</sub> concentrations. Another benefit  
313 of using CO as OHR<sub>ext</sub> source for the estimation of OH<sub>exp</sub> is that it introduces complexity in the precursor, which resembled  
314 those in real applications. Although not tested in this study, we also note that further trace-gas decay experiments in the  
315 presence of N<sub>2</sub>O/NO<sub>x</sub> (typical urban environment) should be conducted when oxidation chemistry in the presence of NO<sub>x</sub> is  
316 studied (Cheng et al., 2021).



317

318 **Figure 3: The regression results of  $OH_{exp, dec}$  and  $OH_{exp, est}$  in the OFR185 mode with (a) SO<sub>2</sub> and (b) CO as  $OHR_{ext}$  sources. (c)**  
 319 **Results from all experiments (using SO<sub>2</sub> and CO) in the OFR185 mode.**

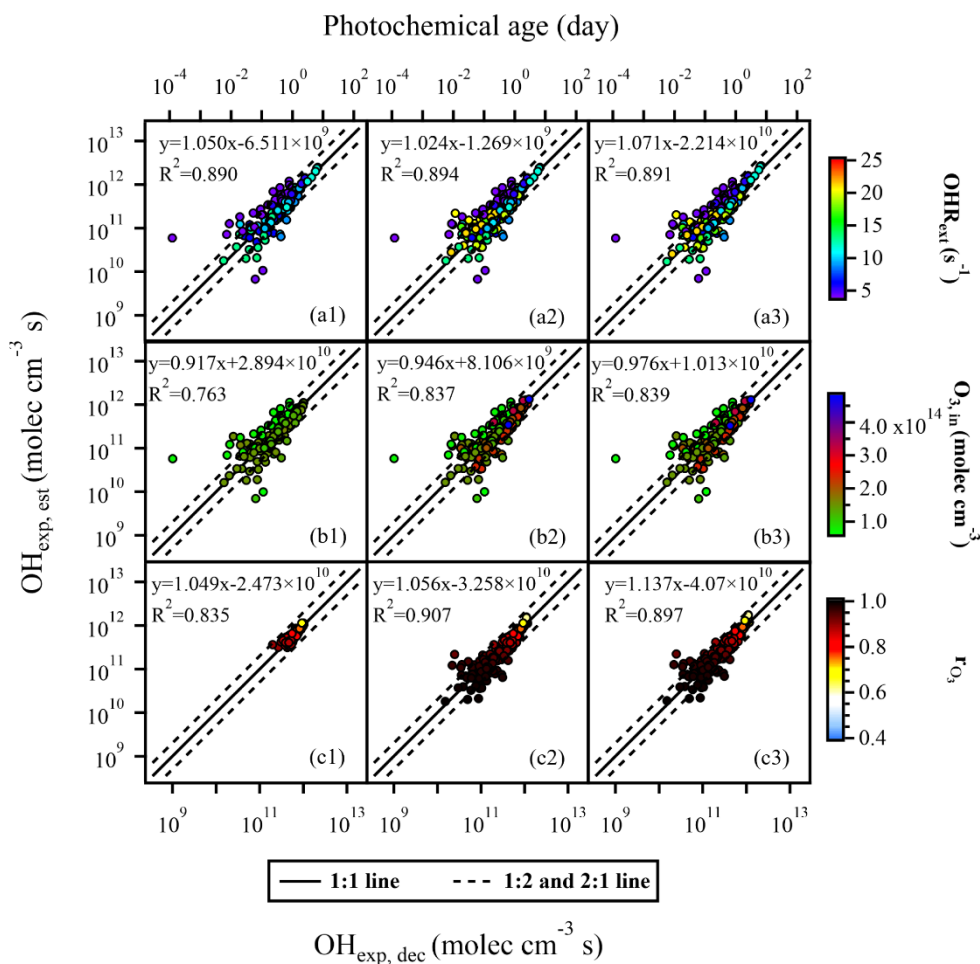
### 320 3.4 The OFR254 mode

321 The equation for  $OH_{exp}$  estimation in OFR254 mode is simpler compared to that of OFR185 mode. According to Eq. 3, under  
 322 OFR254 mode, the three parameters potentially affecting the  $OH_{exp}$  are  $OHR_{ext}$ , input O<sub>3</sub> concentration, and  $r_{O_3}$ . We found that  
 323 compared to Figure 1, the data points in Figure 4 were more scattered. Most of the  $R^2$  values in Figure 4 were below 0.9,  
 324 indicating that using SO<sub>2</sub> as the  $OHR_{ext}$  source, the estimation of  $OH_{exp}$  (using Eq. 3) under the OFR254 mode performed not  
 325 as well as those under the OFR185 mode (using Eq. 2). Firstly, we investigated the impacts of  $OHR_{ext}$ . Figure 4a1 showed the  
 326 regression results of  $OH_{exp, est}$  and  $OH_{exp, dec}$  when  $OHR_{ext}$  ranged from 4.6 to 13.6 s<sup>-1</sup>. The parameters  $a-c$  ( $FP_{IOHR, 254}$ ;  $IOHR$ :  
 327 low external OHR) (Table S4) were obtained by fitting Eq. 3 to  $OH_{exp, dec}$ . In Figure 4a2, the same set of fitted parameters  
 328  $FP_{IOHR, 254}$  from Figure 4a1 were used for a wider range of  $OHR_{ext}$  (4.6–21.2 s<sup>-1</sup>). From the regression results (slopes of 1.050  
 329 and 1.024,  $R^2$  of 0.890 and 0.894), the same set of parameters yielded similar estimation performance for  $OH_{exp}$  despite a wider  
 330 range of  $OHR_{ext}$  in Figure 4a2 compared to that of Figure 4a1. At the same time, these results were not much different from  
 331 those (slope = 1.071,  $R^2$  = 0.891) using a re-fitted set of parameters ( $FP_{eOHR, 254}$ ;  $eOHR$ : extended external OHR) for the wider  
 332 range of  $OHR_{ext}$  (Figure 4a3). Even though the correlation was not as good as those in the OFR185 mode, approximately 85  
 333 % of the data points agreed within a factor of 2. We did not further extend the  $OHR_{ext}$  to values as high as those in the OFR185  
 334 mode as discussed above, since the OFR254 mode was much less oxidative and might not be suitable for simulating the  
 335 oxidation chemistry of extremely high  $OHR_{ext}$  as those from direct emissions.

336 Similarly good correlations were observed when we only used the fitted parameters ( $FP_{IO_3, 254}$  and  $FP_{mrO_3, 254}$ , respectively;  $IO_3$ :  
 337 low O<sub>3, in</sub>,  $mrO_3$ : medium  $r_{O_3}$ ) from narrow ranges of input O<sub>3</sub> concentration and  $r_{O_3}$  (Figure 4b1 and Figure 4c1, respectively)



338 to reconstruct the  $\text{OH}_{\text{exp, est}}$  values with extended ranges of these experimental conditions (Figure 4b2 and Figure 4c2,  
 339 respectively). Such correlations were as good as those with re-fitted parameters ( $\text{FP}_{\text{eO}_3, 254}$  and  $\text{FP}_{\text{erO}_3, 254}$ , respectively;  $\text{eO}_3$ :  
 340 extended  $\text{O}_{3, \text{in}}$ ,  $\text{erO}_3$ : extended  $\text{rO}_3$ ) from data points in the extended ranges of  $\text{O}_3$  concentration and  $\text{rO}_3$  (Figure 4b3 and Figure  
 341 4c3, respectively). These observations thus indicate that under the OFR254 mode, when  $\text{OHR}_{\text{ext}}$ ,  $\text{O}_{3, \text{in}}$ , and  $\text{rO}_3$  vary within  
 342 certain ranges ( $4.6\text{--}21.2 \text{ s}^{-1}$ ,  $6.5 \times 10^{13}\text{--}4.8 \times 10^{14} \text{ molec cm}^{-3}$ , and  $0.61\text{--}0.99$ , respectively), Eq. 3 can be used to estimate  
 343 OH radical levels reasonably well using the fitted parameters ( $a\text{--}c$ ) obtained from a narrower range of data points.

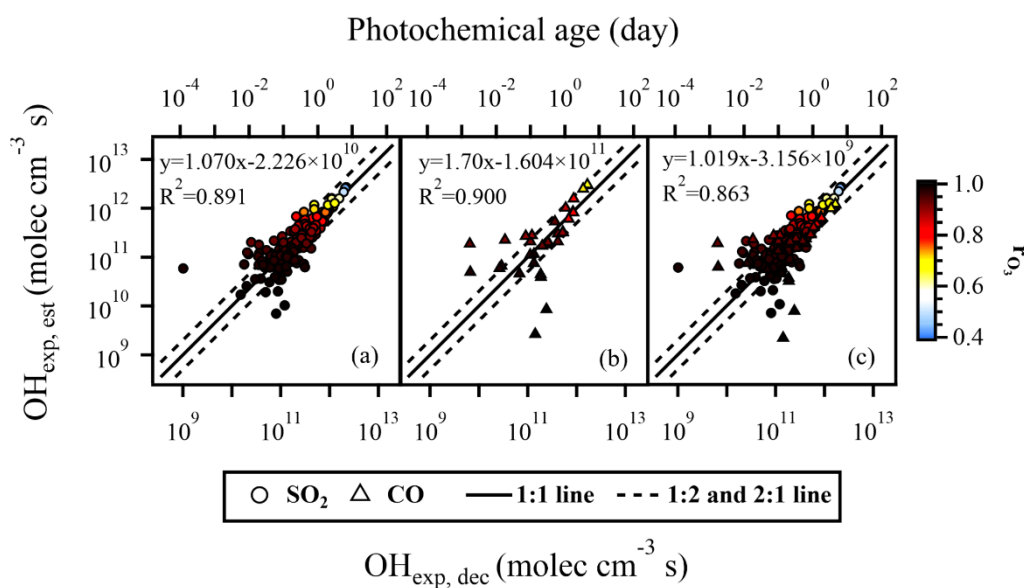


344

345 **Figure 4:** The regression results of  $\text{OH}_{\text{exp, est}}$  and  $\text{OH}_{\text{exp, dec}}$  when variations occurred in (a1–a3)  $\text{OHR}_{\text{ext}}$ , (b1–b3) input  $\text{O}_3$   
 346 concentration, and (c1–c3)  $\text{rO}_3$ . Compared to panels a1, b1, and c1, panels a2, b2, and c2 respectively incorporated additional data  
 347 points with extended  $\text{OHR}_{\text{ext}}$ ,  $\text{O}_{3, \text{in}}$ , and  $\text{rO}_3$  values, but still utilized the fitting parameters  $\text{FP}_{\text{IOHR}, 254}$ ,  $\text{FP}_{\text{IO}_3, 254}$ , and  $\text{FP}_{\text{mrO}_3, 254}$   
 348 obtained from the lower or medium condition range to estimate  $\text{OH}_{\text{exp, est}}$ . In panels a3, b3, and c3, all data points within the extended  
 349 condition range were used to re-fit the parameters  $a\text{--}c$ , and the resulting  $\text{FP}_{\text{eOHR}, 254}$ ,  $\text{FP}_{\text{eO}_3, 254}$ , and  $\text{FP}_{\text{erO}_3, 254}$  were employed to  
 350 estimate  $\text{OH}_{\text{exp, est}}$ .



351 Figure 5a and Figure 5b depicted the correlation between  $\text{OH}_{\text{exp, est}}$  estimated from Eq. 3 and  $\text{OH}_{\text{exp, dec}}$  calculated from Eq. 1  
 352 with  $\text{SO}_2$  and  $\text{CO}$  as  $\text{OHR}_{\text{ext}}$  sources, respectively. When using  $\text{SO}_2$  as the  $\text{OHR}_{\text{ext}}$  source, approximately 86 % of the data  
 353 points agreed within a factor of 2 (Figure 5a). Similar to the case of OFR185, when  $\text{CO}$  was used as the  $\text{OHR}_{\text{ext}}$  source, the  
 354 data points were more scattered, with the percentage of data points within a factor of 2 dropping to only about 64 % (Figure  
 355 5b). Figure 5c included data points using both  $\text{SO}_2$  and  $\text{CO}$  as the  $\text{OHR}_{\text{ext}}$  sources. Overall, regardless of the  $\text{OHR}_{\text{ext}}$  source,  
 356 when  $r_{\text{O}_3}$  was higher than 0.93, which meant a low UV intensity, the majority of data points for  $\text{OH}_{\text{exp, est}}$  and  $\text{OH}_{\text{exp, dec}}$  differed  
 357 by a factor of two or more. It is therefore recommended that when using the OFR254 mode, too low lamp power settings  
 358 should be avoided.



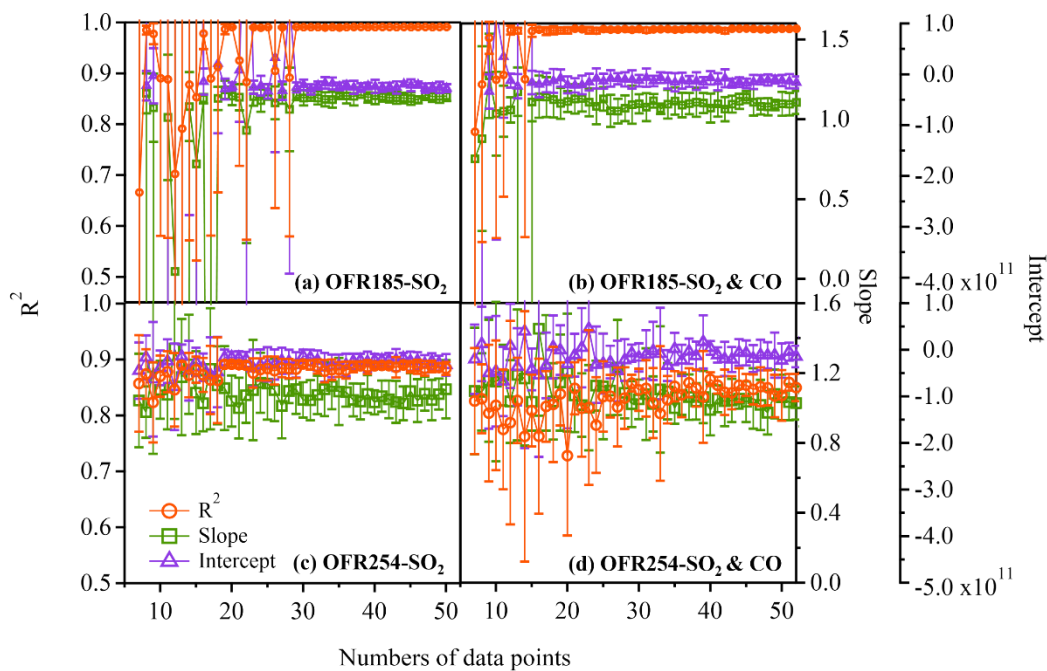
359  
 360 **Figure 5: The regression results of  $\text{OH}_{\text{exp, dec}}$  and  $\text{OH}_{\text{exp, est}}$  in the OFR254 mode with (a)  $\text{SO}_2$  and (b)  $\text{CO}$  as  $\text{OHR}_{\text{ext}}$  sources. (c)**  
 361 **Results from all experiments ( $\text{SO}_2$  and  $\text{CO}$ ) in the OFR254 mode.**

#### 362 4 Conclusions

363 A series of  $\text{OH}_{\text{exp}}$  estimation experiments using the PAM-OFR were conducted in OFR185 and OFR254 modes to explore the  
 364 applicability of the empirical equations under a wide range of conditions. The results indicate that for OFR185 mode, when  
 365 varying the residence time, water vapor mixing ratio, and output  $\text{O}_3$  concentration (as a surrogate for UV intensity) within  
 366 certain ranges, the empirical equation (Eq. 2) for  $\text{OH}_{\text{exp}}$  proves to be effective in estimating  $\text{OH}_{\text{exp}}$ . Unless there is a significant  
 367 change in  $\text{OHR}_{\text{ext}}$ , such as transitioning from ambient conditions to emission source conditions, there is no need to re-fit the  
 368 parameters  $a-f$  in the estimation equation to estimate  $\text{OH}_{\text{exp}}$ . In comparison to OFR185 mode, the consistency between  $\text{OH}_{\text{exp, est}}$   
 369 and  $\text{OH}_{\text{exp, dec}}$  in the OFR254 mode is not as good. For the OFR254 mode, when  $\text{OHR}_{\text{ext}}$ , input  $\text{O}_3$  concentration, and  $r_{\text{O}_3}$  vary  
 370 within certain ranges, the empirical equation (Eq. 3) can be used to estimate  $\text{OH}_{\text{exp}}$  reasonably well using the parameters  $a-c$



371 obtained from a narrower range of data points. It is important to note that for the OFR185 mode, the above conclusions are  
372 valid only if one already has a set of  $a-f$  values that are appropriate for the specific UV lamps being used, as the  $I_{185}:I_{254}$  that  
373 affects the  $\text{OH}_{\text{exp}}$  is lamp-specific. For a PAM-OFR that employs a different Hg lamp, a series of calibration experiments  
374 should be conducted in any case. Alternatively, based on the research by Rowe et al. (2020), the exponential relationship  
375 between the  $a-f$  values and the  $I_{185}:I_{254}$  could be used to first obtain a set of  $a-f$  values suitable for the UV lamps being used.  
376 To obtain reliable estimates of  $\text{OH}_{\text{exp}}$  using Eqs. 2 and 3 for the OFR185 mode or OFR254 mode, respectively, it is desirable  
377 to have sufficient data points (that is,  $\text{OH}_{\text{exp, dec}}$  from trace-gas decay experiments) to fit the parameters for the calculation of  
378  $\text{OH}_{\text{exp, est}}$ . There is currently no consensus on how many data points in trace-gas decay experiments are enough for reliable  
379 fitted parameters, which could be important for in-situ  $\text{OH}_{\text{exp}}$  estimation in field studies where a limited number of experiments  
380 are done to reduce downtime. We aim to address this by random sampling from the data points in our experiments and  
381 determine the minimum number of experiments that are needed to obtain reliable  $\text{OH}_{\text{exp}}$ .  
382 For OFR185 mode, we first used randomly selected  $N$  data points from the 175 data points presented previously to fit the  
383 parameters ( $a-f$ ) using Eq. 2. The fitted parameters were then used to reconstruct  $\text{OH}_{\text{exp, est}}$  for all the 175 data points. The  
384  $\text{OH}_{\text{exp, est}}$  values were then compared with the corresponding 175  $\text{OH}_{\text{exp, dec}}$  values. This procedure was repeated 10 times for  
385 each  $N$ , with  $N$  starting from 7 till approximately 50 (Figure 6a). The average  $R^2$ , slope, and intercept from the 10 attempts  
386 were then shown as a function of  $N$  for experiments with  $\text{SO}_2$  only (Figure 6a) and those with  $\text{SO}_2$  and CO (Figure 6b). It can  
387 be observed that around 30 data points are needed for experiments with  $\text{SO}_2$  only while around 20 data points are needed to  
388 have stable  $R^2$  values and slopes when using both  $\text{SO}_2$  and CO. For OFR254 mode, the same procedure was applied to the 241  
389 data points. It was not surprising that the results were a lot more scattered (Figure 6c and Figure 6d) compared to those for  
390 OFR185 mode given their performance shown in the previous section. Nevertheless, our analysis suggests that around 25 data  
391 points are needed to obtain reliable  $\text{OH}_{\text{exp, est}}$  for OFR254 mode, whether  $\text{SO}_2$  alone (Figure 6c) or  $\text{SO}_2$  and CO (Figure 6d) are  
392 used for the trace-gas decay experiments. Therefore, despite the limitation that this practice only randomly samples the data  
393 points without considering the range of any experimental conditions, our analysis suggests that 20–30 data points are normally  
394 needed to obtain reliable  $\text{OH}_{\text{exp}}$  for both OFR185 and OFR254 modes.



395

396 **Figure 6: The regression results of  $\text{OH}_{\text{exp, dec}}$  and  $\text{OH}_{\text{exp, est}}$  (characterized by the  $R^2$ , slope, and intercept) when different numbers of**  
397 **data points were chosen. (a)  $\text{SO}_2$  as  $\text{OHR}_{\text{ext}}$  source in OFR185 mode, (b)  $\text{SO}_2$  or  $\text{CO}$  as  $\text{OHR}_{\text{ext}}$  source in OFR185 mode, (c)  $\text{SO}_2$  as**  
398  **$\text{OHR}_{\text{ext}}$  source in the OFR254 mode, and (d)  $\text{SO}_2$  or  $\text{CO}$  as  $\text{OHR}_{\text{ext}}$  source in the OFR254 mode.**

399 Our study suggests that the  $\text{OH}_{\text{exp, est}}$  estimated from the empirical equations agrees better with  $\text{OH}_{\text{exp, dec}}$  for the OFR185  
400 (Figure 3) than for the OFR254 mode (Figure 5). This can be understood from the perspective of OH generation and its  
401 consumption by  $\text{OHR}_{\text{ext}}$  (Li et al., 2015). For the OFR185 mode, there are two pathways to generate OH radicals: the photolysis  
402 of  $\text{H}_2\text{O}$  and the photolysis of  $\text{O}_3$ . For the OFR254 mode, the main pathway for OH radical generation is solely the photolysis  
403 of  $\text{O}_3$ . Consequently, when  $\text{OHR}_{\text{ext}}$  changes, the disruption to  $\text{OH}_{\text{exp}}$  in the system is more significant in the case of the OFR254  
404 mode, while the  $\text{OH}_{\text{exp}}$  in the OFR185 mode remains more stable. In addition, pseudo-first-order kinetics between OH radicals  
405 and  $\text{SO}_2$  or  $\text{CO}$  is assumed, with  $[\text{OH}]$  being at a pseudo-steady state. Yet, the relatively low OH radical generation capacity  
406 in the OFR254 mode might not necessarily always fulfil such an assumption, leading to higher uncertainties for estimating  
407  $\text{OH}_{\text{exp}}$ . Therefore, the OFR185 mode offers certain advantages such as relatively high  $\text{OH}_{\text{exp}}$ , more accurate  $\text{OH}_{\text{exp}}$  estimation,  
408 as well as no external input of  $\text{O}_3$  needed. However, for substances that exhibit strong absorption at the wavelength of 185 nm  
409 and are prone to photolysis, such as aromatic species (Peng et al., 2016), using the OFR254 mode is a better choice.

#### 410 Data availability

411 The data shown in the paper are available on request from the corresponding authors (huangdd@saes.sh.cn and  
412 yongjieli@um.edu.mo).





#### 415 **Author contribution**

416 QL, DDH, and YJL conceived and planned the experiments. QL and YW carried out the experiments. QL, DDH, and YJL  
417 analysed the data and took the lead in writing the paper. QL, DDH, YJL, ATL, and XC contributed to the interpretation of the  
418 results. SL, LZ, CYH, ST, QC, KIH, HW, KMM, and CH provided significant input during the revision of the manuscript. All  
419 authors provided feedback on the paper.

#### 420 **Competing interests**

421 The authors declare no competing interests.

#### 422 **Acknowledgements**

423 Dan Dan Huang acknowledges the financial support from the National Key Research and Development Program of China  
424 (2022YFC3703600), the Science and Technology Commission of Shanghai Municipality (21230711000) and the General  
425 Fund of Natural Science Foundation of China (42275124). Yong Jie Li acknowledges the financial support from Science and  
426 Technology Development Fund, Macau SAR (File No. 0031/2023/AFJ and 0107/2023/RIA2) and multiyear research grants  
427 (No. MYRG2022-00027-FST and MYRG-GRG2023-00008-FST-UMDF) from the University of Macau.

#### 428 **References**

429 Atkinson, R. and Arey, J.: Atmospheric degradation of volatile organic compounds, *Chem. Rev.*, 103, 4605-4638, doi:  
430 10.1021/cr0206420, 2003.  
431 Atkinson, R., Baulch, D. L., Cox, R. A., Crowley, J. N., Hampson, R. F., Hynes, R. G., Jenkin, M. E., Rossi, M. J., and Troe,  
432 J.: Evaluated kinetic and photochemical data for atmospheric chemistry: Volume II—gas phase reactions of organic species,  
433 *Atmos. Chem. Phys.*, 6, 3625-4055, doi: 10.5194/acp-6-3625-2006, 2006.  
434 Avery, A. M., Alton, M. W., Canagaratna, M. R., Krechmer, J. E., Sueper, D. T., Bhattacharyya, N., Hildebrandt Ruiz, L.,  
435 Brune, W. H., and Lambe, A. T.: Comparison of the Yield and Chemical Composition of Secondary Organic Aerosol  
436 Generated from the OH and Cl Oxidation of Decamethylcyclopentasiloxane, *ACS Earth and Space Chemistry*, 7, 218-229,  
437 doi: 10.1021/acsearthspacechem.2c00304, 2023.  
438 Burkholder, J. B., Sander, S. P., Abbatt, J. P. D., Barker, J. R., Cappa, C., Crouse, J. D., Dibble, T. S., Huie, R. E., Kolb, C.  
439 E., Kurylo, M. J., Orkin, V. L., Percival, C. J., Wilmouth, D. M., and Wine, P. H.: Chemical kinetics and photochemical data  
440 for use in atmospheric studies, Evaluation Number 19, Pasadena, CA: Jet Propulsion Laboratory, National Aeronautics and  
441 Space Administration, <http://jpldataeval.jpl.nasa.gov>, 2020.



- 442 Cao, J., Wang, Q., Li, L., Zhang, Y., Tian, J., Chen, L. A., Ho, S. S. H., Wang, X., Chow, J. C., and Watson, J. G.: Evaluation  
443 of the oxidation flow reactor for particulate matter emission limit certification, *Atmos. Environ.*, 224, 117086, doi:  
444 10.1016/j.atmosenv.2019.117086, 2020.
- 445 Cheng, X., Chen, Q., Jie Li, Y., Zheng, Y., Liao, K., and Huang, G.: Highly oxygenated organic molecules produced by the  
446 oxidation of benzene and toluene in a wide range of OH exposure and NO<sub>x</sub> conditions, *Atmos. Chem. Phys.*, 21, 12005-12019,  
447 doi: 10.5194/acp-21-12005-2021, 2021.
- 448 Cheng, X., Li, Y. J., Zheng, Y., Liao, K., Koenig, T. K., Ge, Y., Zhu, T., Ye, C., Qiu, X., and Chen, Q.: Oxygenated organic  
449 molecules produced by low-NO<sub>x</sub> photooxidation of aromatic compounds: contributions to secondary organic aerosol and steric  
450 hindrance, *Atmos. Chem. Phys.*, 24, 2099-2112, doi: 10.5194/acp-24-2099-2024, 2024.
- 451 Clerc, M. and Barat, F.: Kinetics of CO formation studied by far-UV flash photolysis of CO<sub>2</sub>, *J. Chem. Phys.*, 46, 107-110,  
452 doi: 10.1063/1.1840358, 1967.
- 453 Cocker, D. R., Flagan, R. C., and Seinfeld, J. H.: State-of-the-art chamber facility for studying atmospheric aerosol chemistry,  
454 *Environ. Sci. Technol.*, 35, 2594-2601, doi: 10.1021/es0019169, 2001.
- 455 Cohen, N. and Heicklen, J.: The Oxidation of Inorganic Non-metallic Compounds, in: *Reactions of Non-Metallic Inorganic*  
456 *Compounds, Compr. Chem. Kinet.*, 1-137, doi: 10.1016/s0069-8040(08)70303-0, 1972.
- 457 Ehhalt, D. H.: Photooxidation of trace gases in the troposphere Plenary Lecture, *Phys. Chem. Chem. Phys.*, 1, 5401-5408, doi:  
458 10.1039/A905097C, 1999.
- 459 Friedman, B. and Farmer, D. K.: SOA and gas phase organic acid yields from the sequential photooxidation of seven  
460 monoterpenes, *Atmos. Environ.*, 187, 335-345, doi: 10.1016/j.atmosenv.2018.06.003, 2018.
- 461 Fuchs, H., Tan, Z., Lu, K., Bohn, B., Broch, S., Brown, S. S., Dong, H., Gomm, S., Häsel, R., and He, L.: OH reactivity at a  
462 rural site (Wangdu) in the North China Plain: contributions from OH reactants and experimental OH budget, *Atmos. Chem.*  
463 *Phys.*, 17, 645-661, doi: 10.5194/acp-17-645-2017, 2017.
- 464 George, I. J., Vlasenko, A., Slowik, J. G., Broekhuizen, K., and Abbatt, J. P. D.: Heterogeneous oxidation of saturated organic  
465 aerosols by hydroxyl radicals: uptake kinetics, condensed-phase products, and particle size change, *Atmos. Chem. Phys.*, 7,  
466 4187-4201, doi: 10.5194/acp-7-4187-2007, 2007.
- 467 Hildebrandt, L., Donahue, N. M., and Pandis, S. N.: High formation of secondary organic aerosol from the photo-oxidation of  
468 toluene, *Atmos. Chem. Phys.*, 9, 2973-2986, doi: 10.5194/acp-9-2973-2009, 2009.
- 469 Kang, E., Root, M. J., Toohey, D. W., and Brune, W. H.: Introducing the concept of potential aerosol mass (PAM), *Atmos.*  
470 *Chem. Phys.*, 7, 5727-5744, doi: 10.5194/acp-7-5727-2007, 2007.
- 471 Lambe, A. T., Ahern, A. T., Williams, L. R., Slowik, J. G., Wong, J. P. S., Abbatt, J. P. D., Brune, W. H., Ng, N. L., Wright,  
472 J. P., and Croasdale, D. R.: Characterization of aerosol photooxidation flow reactors: heterogeneous oxidation, secondary  
473 organic aerosol formation and cloud condensation nuclei activity measurements, *Atmos. Meas. Tech.*, 4, 445-461, doi:  
474 10.5194/amt-4-445-2011, 2011.
- 475 Li, R., Palm, B. B., Ortega, A. M., Hlywiak, J., Hu, W., Peng, Z., Day, D. A., Knote, C., Brune, W. H., and De Gouw, J. A.:  
476 Modeling the radical chemistry in an oxidation flow reactor: Radical formation and recycling, sensitivities, and the OH  
477 exposure estimation equation, *J. Phys. Chem. A*, 119, 4418-4432, doi: 10.1021/jp509534k, 2015.
- 478 Liao, K., Chen, Q., Liu, Y., Li, Y. J., Lambe, A. T., Zhu, T., Huang, R.-J., Zheng, Y., Cheng, X., and Miao, R.: Secondary  
479 organic aerosol formation of fleet vehicle emissions in China: Potential seasonality of spatial distributions, *Environ. Sci.*  
480 *Technol.*, 55, 7276-7286, doi: 10.1021/acs.est.0c08591, 2021.
- 481 Liu, J., Chu, B., Chen, T., Liu, C., Wang, L., Bao, X., and He, H.: Secondary organic aerosol formation from ambient air at an  
482 urban site in Beijing: effects of OH exposure and precursor concentrations, *Environ. Sci. Technol.*, 52, 6834-6841, doi:  
483 10.1021/acs.est.7b05701, 2018.
- 484 Lou, S., Holland, F., Rohrer, F., Lu, K., Bohn, B., Brauers, T., Chang, C. C., Fuchs, H., Häsel, R., and Kita, K.: Atmospheric  
485 OH reactivities in the Pearl River Delta–China in summer 2006: measurement and model results, *Atmos. Chem. Phys.*, 10,  
486 11243-11260, doi: 10.5194/acp-10-11243-2010, 2010.
- 487 Lu, K., Zhang, Y., Su, H., Brauers, T., Chou, C. C., Hofzumahaus, A., Liu, S. C., Kita, K., Kondo, Y., and Shao, M.: Oxidant  
488 (O<sub>3</sub> + NO<sub>2</sub>) production processes and formation regimes in Beijing, *J. Geophys. Res.: Atmospheres*, 115, doi:  
489 10.1029/2009JD012714, 2010.



- 490 Mao, J., Ren, X., Brune, W. H., Olson, J. R., Crawford, J. H., Fried, A., Huey, L. G., Cohen, R. C., Heikes, B., and Singh, H.  
491 B.: Airborne measurement of OH reactivity during INTEX-B, *Atmos. Chem. Phys.*, 9, 163-173, doi: org/10.5194/acp-9-163-  
492 2009, 2009.
- 493 Nakashima, Y., Kamei, N., Kobayashi, S., and Kajii, Y.: Total OH reactivity and VOC analyses for gasoline vehicular exhaust  
494 with a chassis dynamometer, *Atmos. Environ.*, 44, 468-475, doi: 10.1016/j.atmosenv.2009.11.006, 2010.
- 495 Ono, R., Nakagawa, Y., Tokumitsu, Y., Matsumoto, H., and Oda, T.: Effect of humidity on the production of ozone and other  
496 radicals by low-pressure mercury lamps, *J Photochem Photobiol, A*, 274, 13-19, doi: 10.1016/j.jphotochem.2013.09.012, 2014.
- 497 Peng, Z. and Jimenez, J. L.: KinSim: a research-grade, user-friendly, visual kinetics simulator for chemical-kinetics and  
498 environmental-chemistry teaching, *J. Chem. Educ.*, 96, 806– 811, doi: 10.1021/acs.jchemed.9b00033, 2019.
- 499 Peng, Z. and Jimenez, J. L.: Radical chemistry in oxidation flow reactors for atmospheric chemistry research, *Chem. Soc. Rev.*,  
500 49, 2570-2616, doi: 10.1039/C9CS00766K, 2020.
- 501 Peng, Z., Day, D. A., Stark, H., Li, R., Lee-Taylor, J., Palm, B. B., Brune, W. H., and Jimenez, J. L.: HO<sub>x</sub> radical chemistry  
502 in oxidation flow reactors with low-pressure mercury lamps systematically examined by modeling, *Atmos. Meas. Tech.*, 8,  
503 4863-4890, doi: 10.5194/amt-8-4863-2015, 2015.
- 504 Peng, Z., Day, D. A., Ortega, A. M., Palm, B. B., Hu, W., Stark, H., Li, R., Tsigaridis, K., Brune, W. H., and Jimenez, J. L.:  
505 Non-OH chemistry in oxidation flow reactors for the study of atmospheric chemistry systematically examined by modeling,  
506 *Atmos. Chem. Phys.*, 16, 4283-4305, doi: 10.5194/acp-16-4283-2016, 2016.
- 507 Rowe, J. P., Lambe, A. T., and Brune, W. H.: Effect of varying the  $\lambda=185$  and 254 nm photon flux ratio on radical generation  
508 in oxidation flow reactors, *Atmos. Chem. Phys.*, 20, 13417-13424, doi: 10.5194/acp-20-13417-2020, 2020.
- 509 Seinfeld, J. H. and Pandis, S. N.: *Atmospheric chemistry and physics: from air pollution to climate change*, John Wiley &  
510 Sons, Inc., ISBN 9781119221166, 2016.
- 511 Stone, D., Whalley, L. K., and Heard, D. E.: Tropospheric OH and HO<sub>2</sub> radicals: field measurements and model comparisons,  
512 *Chem. Soc. Rev.*, 41, 6348-6404, doi: 10.1039/C2CS35140D, 2012.
- 513 Tan, Z., Fuchs, H., Lu, K., Hofzumahaus, A., Bohn, B., Broch, S., Dong, H., Gomm, S., Häsel, R., and He, L.: Radical  
514 chemistry at a rural site (Wangdu) in the North China Plain: observation and model calculations of OH, HO<sub>2</sub> and RO<sub>2</sub> radicals,  
515 *Atmos. Chem. Phys.*, 17, 663-690, doi: 10.5194/acp-17-663-2017, 2017.
- 516 Tan, Z., Rohrer, F., Lu, K., Ma, X., Bohn, B., Broch, S., Dong, H., Fuchs, H., Gkatzelis, G. I., and Hofzumahaus, A.:  
517 Wintertime photochemistry in Beijing: observations of RO<sub>x</sub> radical concentrations in the North China Plain during the BEST-  
518 ONE campaign, *Atmos. Chem. Phys.*, 18, 12391-12411, doi: 10.5194/acp-18-12391-2018, 2018.
- 519 Wang, N., Zannoni, N., Ernle, L., Bekö, G., Wargocki, P., Li, M., Weschler, C. J., and Williams, J.: Total OH reactivity of  
520 emissions from humans: in situ measurement and budget analysis, *Environ. Sci. Technol.*, 55, 149-159, doi:  
521 10.1021/acs.est.0c04206, 2020.
- 522 Wang, X., Liu, T., Bernard, F., Ding, X., Wen, S., Zhang, Y., Zhang, Z., He, Q., Lü, S., and Chen, J.: Design and  
523 characterization of a smog chamber for studying gas-phase chemical mechanisms and aerosol formation, *Atmos. Meas. Tech.*,  
524 7, 301-313, doi: 10.5194/amt-7-301-2014, 2014.
- 525 Yang, Y., Shao, M., Keßel, S., Li, Y., Lu, K., Lu, S., Williams, J., Zhang, Y., Zeng, L., and Nölscher, A. C.: How the OH  
526 reactivity affects the ozone production efficiency: case studies in Beijing and Heshan, China, *Atmos. Chem. Phys.*, 17, 7127-  
527 7142, doi: 10.5194/acp-17-7127-2017, 2017.
- 528 You, X., Wang, H., Goos, E., Sung, C.-J., and Klippenstein, S. J.: Reaction kinetics of CO + HO<sub>2</sub> → products: ab initio  
529 transition state theory study with master equation modeling, *J. Phys. Chem. A*, 111, 4031-4042, doi: 10.1021/jp067597a, 2007.
- 530 Zhang, Z., Xu, W., Lambe, A. T., Hu, W., Liu, T., and Sun, Y.: Insights Into Formation and Aging of Secondary Organic  
531 Aerosol From Oxidation Flow Reactors: A Review, *Curr. Pollut. Rep.*, 1-14, doi: 10.1007/s40726-024-00309-7, 2024.
- 532